Cotunneling spectroscopy and the properties of excited-state spin manifolds of Mn_{12} single molecule magnets

Fatemeh Rostamzadeh Renani and George Kirczenow
Department of Physics, Simon Fraser University, Burnaby, British Columbia, Canada V5A 1S6
(Received 31 July 2014; published 14 October 2014)

We study charge transport through single molecule magnet (SMM) junctions in the cotunneling regime as a tool for investigating the properties of the excited-state manifolds of neutral Mn_{12} SMs. This study is motivated by a recent transport experiment [S. Kahle *et al.*, Nano Lett. **12**, 518 (2012)] that probed the details of the magnetic and electronic structure of Mn_{12} SMMs beyond the ground-state spin manifold. A giant spin Hamiltonian and master equation approach is used to explore theoretically the cotunneling transport through Mn_{12}-Ac SMM junctions. We identify SMM transitions that can account for both the strong and weak features of the experimental differential conductance spectra. We find the experimental results to imply that the excited spin-state manifolds of the neutral SMM have either different anisotropy constants or different g factors in comparison with its ground-state manifold. However, the latter scenario accounts best for the experimental data.

DOI: 10.1103/PhysRevB.90.165118 PACS number(s): 73.63.−b, 75.50.Xx, 73.23.Hk

I. INTRODUCTION

Integrating the electronic spin and charge on the molecular scale is the main idea behind the active field of molecular spintronics. A practical goal of molecular spintronics is the further minimization of the electronic components. Because of their large magnetic anisotropy barriers and associated stable magnetic moments, single molecule magnets (SMMs) bring a new dimension to this field and also raise the possibility of molecular magnetic information storage and quantum computation. Therefore the transport properties of two- and three-terminal devices based on individual SMMs are attracting considerable experimental [1–5] and theoretical [6–19] interest at present.

Mn_{12} is the the first discovered [20] and most studied SMM. The large ground state spin $S = 10$ [21] and large magnetic anisotropy barrier (up to $\sim$6.1 meV along the easy axis) [22] lead to high blocking temperatures ($\sim$3.5 K) [23] and long relaxation times [24]. Experimental results have demonstrated that an individual Mn_{12} SMM can be addressed electronically and therefore SMMs have potential applications such as storing information. Three main theoretical approaches have been adopted in studying transport through individual SMMs: giant spin Hamiltonian (GSH) models [6–10], density functional theory (DFT) based calculations [11–16], and tight binding (TB) models [17–19]. The GSH-based models are the simplest, being formulated entirely in terms of the operator describing the total electronic spin of the SMM, whereas the DFT and TB models also take the spatial part of the electronic state as well as the spin states of the individual electrons of the SMM explicitly into account. However, models based on the GSH have yielded many important insights into the behavior of these systems. They have the advantages of their conceptual simplicity and of the transparency of the results that they yield.

The single spin manifold ($S = 10$) picture is sufficient to explain many experimental properties of the Mn_{12}-Ac SMM. However, it has been suggested (based on experiments) [25,26] and predicted by DFT-based calculations [27] that the neutral Mn_{12} SMM has excited-state manifolds which have slightly higher energies than the ground-state manifold. The first excited-state manifold of the neutral Mn_{12} SMM has been estimated to locate 4 meV above its ground-state manifold and to have $S_{tot} = 9$ [25–27]. Therefore the anisotropy barrier of the first excited-state manifold of the neutral Mn_{12} SMM overlaps with the anisotropy barrier of the ground-state manifold which can affect the transport properties of SMM transistors (SMMs). However, the properties of the low-lying excited manifolds are still not well understood.

Electronic tunneling experiments on SMMs can provide valuable information regarding both the ground- and excited-state manifolds. In the Coulomb blockade regime where the effects of the charging energy of the SMM on transport are not overcome by the applied bias or gate voltages, transport is mediated by virtual states, a process referred to as "cotunneling.. The cotunneling process may be elastic or inelastic. Inelastic cotunneling happens when the final state of the individual molecule differs from its initial state after a cotunneling process. Inelastic cotunneling spectroscopy can provide valuable information about the electronic, magnetic, and vibrational excitations of the SMM coupled to the electrodes. In particular, the positions of conductance peaks are a very direct fingerprint of the excitation spectrum of this system.

Recently, inelastic cotunneling experiments carried out by Kahle *et al.* [5] have probed the details of the magnetic and electronic structure of a Mn_{12} SMM in different spin-state manifolds and also within each spin-state manifold. The SMM was separated from a metal substrate electrode by a thin insulating layer and contacted by a second electrode in the form of a scanning tunneling microscope tip. In this study three main features were observed in the differential conductance spectra. These features were attributed [5] to spin-flip excitations within the Mn_{12} SMM and to excitations involving more than one spin-state manifold of the Mn_{12} SMM. The application of an external magnetic field was found to raise the bias voltage at which the first excitation in the differential conductance measurements was observed [5]. However, the magnetic field lowered the bias voltages at which the higher-energy excitations occurred [5]. Although a phenomenological eight-spin model with parameters estimated from DFT-based calculations supported the observation of such features [5], it did not explain the opposite behaviors of the excitations under the applied magnetic field. Whether this shortcoming of

the modeling presented in Ref. [5] was due to an inadequacy of the eight-spin model phenomenology or to the well-known limitations of DFT for excited-state calculations [28] is unclear at this time. To our knowledge, no relevant quantitative theory has as yet been reported accounting for this behavior. Thus the physics responsible for the observed novel behavior has not been identified.

In this paper we present a theory of cotunneling in Mn_{12} SMMs that takes into account the ground and first excited spin manifolds. We then investigate possible mechanisms that may account for the previously unexplained behavior observed in Kahle's recent experiment [5]. In the present theory we adopt the GSH model of the SMM electronic and spintronic states. We evaluate the differential conductance of the SMM in the cotunneling transport regime by solving the appropriate master equations, and evaluating the relevant transition rates perturbatively since the system of interest is in the weak tunneling regime. We find the strongest features in the cotunneling spectra of Kahle *et al.* [5] to arise from transitions from the ground state of the ground-state spin manifold of the SMM to other states of the ground-state manifold and states of exited manifolds. We suggest that transitions from excited states of the ground-state manifold give rise to the weaker features in the cotunneling spectra of Kahle *et al.* [5] that were not accounted for by the modeling presented in Ref. [5]. We propose different possible mechanisms that can account for the opposite behaviors of the low energy excitations of the Mn_{12} SMM under applied magnetic fields that were observed by Kahle *et al.* [5]. Of these the one that we find to account best for the experimental data requires the different spin manifolds of the neutral SMM to have differing g factors and that the magnetic field be approximately parallel to the SMM's magnetic easy axis.

II. THEORY

The SMM device under consideration can be divided into the left and right electrodes and a central molecule. Thus, the Hamiltonian for the entire system is written as

$$H = H^{\mathrm{SMM}} + H^{L} + H^{R} + H^{T}. \tag{1}$$

Here H^{SMM} is the Hamiltonian of the SMM, $H_{R(L)} = \sum_k \epsilon_{R(L),k} a^{\dagger}_{R(L),k} a_{R(L),k}$ is the Hamiltonian of the right (left) electrode, where $a^{\dagger}$ and a are the creation and annihilation operators of the electrons in electrodes, and $H^{T} = \sum_{k,k'} (t_{R(L);k,k'} a^{\dagger}_{R(L),k} d_{k'} + \mathrm{H.c.})$ describes the tunneling between the SMM and the electrodes; here $d^{\dagger}$ and d are the creation and annihilation operators for electrons in the SMM.

The giant spin Hamiltonian of the SMM is given by

$$H^{\mathrm{SMM}} = -DS_z^2 + g\mu_B \mathbf{B}\cdot\mathbf{S} + \epsilon_0 n, \tag{2}$$

where D is the zero-field uniaxial anisotropy constant. We do not consider the effects of transverse anisotropy here since for Mn_{12} SMMs its contribution to the energy has been shown [29] to be much smaller than that of the uniaxial anisotropy and also much smaller than the thermal energy kT in the experiment of Kahle *et al.* [5]. g is the SMM's g factor, μ_B is the Bohr magneton, $\mathbf{B}$ is the external magnetic field, and ϵ_0 is the on-site energy of the electron in the SMM. n is the number operator, with eigenvalues $n = 0$ for the neutral molecule and $n = 1$ for the negatively charged molecule. $\mathbf{S}$ is the total molecular spin operator. We note that the charge on the SMM in its ground state in the experiment of Kahle *et al.* [5] is not known definitively. However, the predictions of the GSH model for transport in the cotunneling regime do not depend qualitatively on whether the ground state is neutral ($n = 0$), as is assumed here, or carries a positive or negative charge. The same is true whether the virtual state in the cotunneling process is positively or negatively charged relative to the ground state. However, we do not consider virtual states in which the SMM carries a double (or larger) charge relative to the ground state since processes involving such virtual states would contribute to transport in higher orders of perturbation theory than the cotunneling processes that we consider. They are therefore expected to have a much weaker effect on transport than these cotunneling processes.

As will be seen below, the features that appear in the cotunneling spectra of the SMM and their behavior in the presence of applied magnetic fields depend on the values of the anisotropies D and g factors for the various spin manifolds of the SMM that appear in the giant spin Hamiltonian [Eq. (2)] and on the orientation of the magnetic field $\mathbf{B}$ relative to the magnetic easy axis. In Sec. III, we shall explore how each of these parameters influences the calculated cotunneling spectra, and compare these theoretical predictions to the results of the experiment of Kahle *et al.* [5] in order to gain insight into the possible mechanisms underlying the previously unexplained aspects of the experimental data.

The experiment of Kahle *et al.* [5] that we consider here was carried out in the cotunneling regime. In that regime the electron transport through the molecule is mediated by a virtual charged intermediate state of the molecule. For example, in the cotunneling process an electron may tunnel from one of the electrodes to the molecule and from the molecule to the other electrode, the charged intermediate state of the molecule being the virtual state. Because the total energy of the system with the molecule in the charged virtual state may differ from that of the system in its initial and final states, cotunneling can occur at much lower bias voltages applied across the molecule than does sequential tunneling in which the total energy of the system with the added electron on the molecule must equal that of the system before the electron has tunneled to the molecule.

The electron current in the cotunneling regime is given by

$$I = -e \sum_{n,m} \left(R_{LR}^{(2)0,n\to 0,m} - R_{RL}^{(2)0,n\to 0,m} \right) P^{0,n},$$

where $P^{0,n}$ is the occupation probability of the nth state of the neutral SMM and $R^{(2)}_{LR}$ ($R^{(2)}_{RL}$) is the tunneling rate for tunneling events in which an electron transfers from the left (right) electrode to the right (left) electrode. $R^{(2)0,n\to 0,m}$ is given by

$$R_{\alpha\alpha'}^{(2)0,n\to 0,m} = \frac{2\pi}{\hbar}\gamma_\alpha\gamma_{\alpha'} \int_{-\infty}^{+\infty} d\epsilon \left| \sum_{n'} \frac{d_{m,n'} d^{\dagger}_{n',n}}{\epsilon + \epsilon_n - \epsilon_{n'} + i\eta} \right|^2 \times f(\epsilon - \mu_\alpha)[1 - f(\epsilon + \epsilon_n - \epsilon_m - \mu_{\alpha'})].$$

Here $d^{\dagger}_{n';n} = \langle \mathrm{SMM}_{Q=-1,n'} | d^{\dagger} | \mathrm{SMM}_{Q=0,n} \rangle$ is the overlap matrix element, f is the Fermi function distribution, ϵ_n is the

energy of the nth state of the neutral SMM, and μ_α is the electrochemical potential of the α electrode. $\gamma^\alpha = |t_\alpha|^2$ is the square amplitude of the coupling between the α electrode and the SMM.

The occupation probabilities, P, are commonly calculated by solving the master equations,

$$\frac{dP^{0,n}}{dt} = -\sum_m P^{0,n} R^{0,n\to 0,m} + \sum_m P^{0,m} R^{0,m\to 0,n}, \quad (3)$$

where $R^{0,n\to 0,m} = \sum_{\alpha,\alpha'} R^{0,n\to 0,m}_{\alpha\alpha'}$. The first term on the right-hand side gives the rate at which the state $|\mathrm{SMM}_{0,n}\rangle$ decays. This term is proportional to the probability that the system is in the state $|\mathrm{SMM}_{0,n}\rangle$, $P^{0,n}$, multiplied by the rate at which the state decays to other states such as $|\mathrm{SMM}_{0,m}\rangle$. The second term on the right-hand side gives the rate at which the system decays from other states into the $|\mathrm{SMM}_{0,n}\rangle$ state.

In the following section the details of the cotunneling transport through the Mn_{12} SMM junction in the weak coupling regime are investigated.

III. COTUNNELING THROUGH THE Mn_{12} SMM

In the following discussion, for simplicity, it is assumed that the SMM is in its neutral charge state and has two manifolds. The ground-state manifold of the neutral SMM has $S^{\mathrm{g}}_{\mathrm{tot}} = 10$ and its first-excited manifold has $S^{\mathrm{e}}_{\mathrm{tot}} = 9$ and is located 4 meV above its ground-state manifold in the absence of external magnetic fields. It is also assumed that the negatively charged SMM has only one manifold ($S^{\mathrm{anion}}_{\mathrm{tot}} = 9\frac{1}{2}$). The SMM states of the different manifolds are represented by the Dirac notation $|S^{\mathrm{tot}}, S_z\rangle$.

Our goal is to determine whether this theoretical framework within the GSH model can account for the the opposite behaviors of the low energy excitations of the Mn_{12} SMM under applied magnetic fields that were observed by Kahle *et al.* [5]. We begin by focusing on the strongest features that Kahle *et al.* [5] observed in the differential conductance spectra. The GSH model that we consider is characterized by the anisotropy parameter D and g factor that appear in the Hamiltonian [Eq. (2)] for each spin manifold. We consider first in Sec. III A the spectra that are obtained if it is assumed that all of the spin manifolds have the same anisotropy constants D and the same magnetic g factors. Then in Sec. III B we examine the possibility of manifolds with differing anisotropies. This is followed by a discussion in Sec. III C of the results for manifolds with differing g factors. Finally in Sec. III D we discuss the possible origin of the weak features observed by Kahle *et al.* [5] in between the main peaks of the differential conductance spectra at zero magnetic field, and why these features are not visible at high magnetic fields.

A. Spin manifolds with the same anisotropies and g factors

In molecular junction experiments at the onset of a cotunneling process with increasing bias voltage, a new channel for transport opens giving rise to a steplike feature in the differential conductance ($\frac{dI}{dV}$), which corresponds to a peak in the second derivative of the current ($\frac{d^2I}{dV^2}$). In this paper, we have chosen to present our transport results as $\frac{d^2I}{dV^2}$ plots to facilitate comparison with the experimental data presented in Ref. [5].

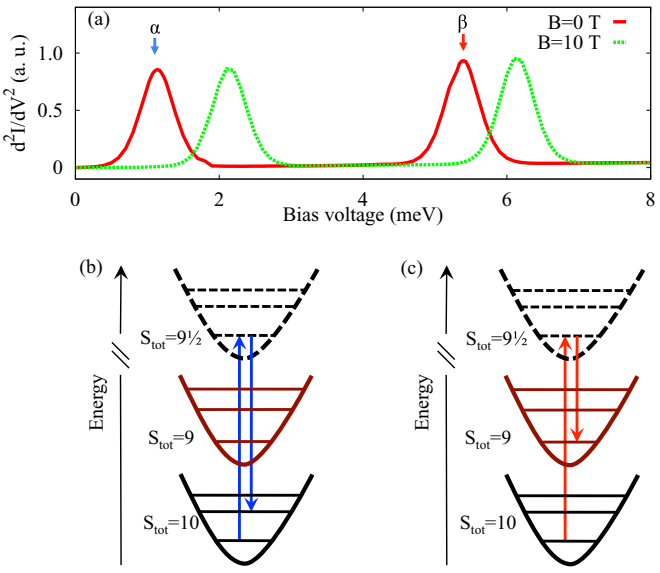

FIG. 1. (Color online) Second derivative of the current, $\frac{d^2I}{dV^2}$, through the Mn_{12} SMM as a function of the bias voltage calculated based on the GSH. All of the spin manifolds have the same anisotropy constants D and magnetic g factors. The red (green) curve represents $\frac{d^2I}{dV^2}$ at the applied magnetic field $B = 0$ T ($B = 10$ T parallel to the SMM easy axis). The parameters of the GSH are $S^{\mathrm{g}}_{\mathrm{tot}} = 10$, $S^{\mathrm{e}}_{\mathrm{tot}} = 9$, $D^{\mathrm{g}}/\hbar^2 = D^{\mathrm{e}}/\hbar^2 = 0.06$ meV, $\epsilon_0 = 1$ eV, $T = 1.5$ K, $g^{\mathrm{g}} = g^{\mathrm{e}} = 2$, and $\gamma_R/\gamma_L = 10^{-4}$. (b), (c) Schematic diagram representing the energies of the two manifolds of the neutral SMM ($S_{\mathrm{tot}} = 10$ and $S_{\mathrm{tot}} = 9$) and negatively charged SMM. (b) The blue arrows show the inelastic cotunneling processes within the ground-Ðstate manifold. The electron tunnels into the SMM which is in its ground state of the ground-state manifold, $|10,10\rangle$, and tunnels out of the SMM leaving the SMM in its first excited state of the ground-state manifold, $|10,9\rangle$. This transport process is mediated by the ground state of the ground-state manifold $|9\frac{1}{2},9\frac{1}{2}\rangle$ of the negatively charged SMM that is the virtual state. Transitions mediated by states in the $S = 9$ manifold do not occur because the $S = 9$ manifold has the same charge as the $S = 10$ manifold and therefore cannot be an intermediate (virtual) state in the cotunneling process. (c) The red arrows show the inelastic cotunneling processes between the two manifolds of the neutral SMM. The electron tunnels into the SMM which is initially in its ground state of the ground-state manifold, $|10,10\rangle$, and tunnels out of the SMM leaving the SMM in its ground state of the first-excited manifold, $|9,9\rangle$. This process is mediated by the ground state of the ground–state manifold $|9\frac{1}{2},9\frac{1}{2}\rangle$ of the negatively charged SMM as the virtual state. The direct transition from the $|10,10\rangle$ state to the $|9,9\rangle$ state is expected to have a lower probability since it would involve direct tunneling of an electron from one electrode to the other, effectively via the vacuum level instead of making use of virtual molecular states that are at lower energies.

Figure 1(a) shows the calculated second derivative of the current, $\frac{d^2I}{dV^2}$, for the Mn_{12} SMM as a function of the bias voltage at zero and $B = 10$ T magnetic field assuming that all of the spin manifolds have the same anisotropy constants D and magnetic g factors. The first calculated peak [indicated by the blue arrow (labeled α) in Fig. 1(a)] corresponds to the inelastic cotunneling within the ground-state manifold. At this

bias voltage an electron tunnels into the SMM which is in its ground state of the ground-state manifold, $|10,10\rangle$, and tunnels out of the SMM leaving the SMM in its first excited state of the ground-state manifold, $|10,9\rangle$ [see Fig. 1(b)]. This bias voltage is enough to overcome the energy difference ($\Delta_{|10,10\rangle,|10,9\rangle}$) between the SMM initial state (the ground state of the ground-state manifold, $|10,10\rangle$) and the SMM final state (the first excited state of the ground-state manifold, $|10,9\rangle$).

Since the energy difference between the ground state and the first excited state of the ground-state manifold, $\Delta_{|10,10\rangle,|10,9\rangle}$, is the largest energy difference between all of the adjacent energy levels of the ground-state manifold, all of the possible elastic and inelastic cotunneling processes *within the ground-state manifold* will begin to happen concurrently at this bias voltage. Therefore, only one $\frac{d^2I}{dV^2}$ peak represents the inelastic cotunneling processes within the ground-state manifold. Our choice of coupling parameters ($\gamma_R/\gamma_L = 10^{-4}$) implies that the ground state of the ground-state manifold remains the dominantly occupied state, although, the excited states are all energetically available.

As illustrated schematically in Fig. 1(c), at the bias voltage of the second peak in Fig. 1(a) [indicated by the red arrow (labeled β)] an electron tunnels into the SMM which is initially in its ground state of the ground-state manifold, $|10,10\rangle$, and tunnels out of the SMM leaving the SMM in its ground state of the first-excited manifold, $|9,9\rangle$ ($|10,10\rangle \rightarrow |9,9\rangle$). Note that transitions from excited states of the ground-state manifold to the excited-manifold states are possible at lower bias voltage than the $|10,10\rangle \rightarrow |9,9\rangle$ transition. However, for the choice of coupling parameters ($\gamma_R/\gamma_L = 10^{-4}$) in Fig. 1(a) the excited states of the ground-state manifold are not significantly occupied as explained above. For this reason these transitions do not result in visible features in Fig. 1(a). Their possible role in the experimental spectra of Kahle *et al.* [5] will be discussed in Sec. III D.

The green curve in Fig. 1(a) shows the effect of the magnetic field applied parallel to the SMM easy axis on the second derivative of the current. As can be seen in this figure, under the applied magnetic field both of the peaks in the $\frac{d^2I}{dV^2}$ plot are shifted to higher bias voltages, contrary to what was observed experimentally [5].

When the applied magnetic field is parallel to the SMM easy axis, S_z is still a good quantum number for the SMM giant spin Hamiltonian. If the applied magnetic field is parallel to the z axis and D and g are the same in the initial and final states the energy differences between the initial and final states of the neutral SMM can be written as

$$\Delta_{\text{initial,final}} \propto \left(-DS_z^2 + g\mu_B \mathbf{B}\cdot\mathbf{S}\right)_{\text{final}} - \left(-DS_z^2 + g\mu_B \mathbf{B}\cdot\mathbf{S}\right)_{\text{initial}} \propto B_z \Delta S_z. \quad (4)$$

The energy difference between the initial and final states of the SMM plays an important role in the cotunneling calculation, because it sets the bias voltage at which inelastic cotunneling may happen. According to Eq. (4), the energy differences $\Delta_{|10,10\rangle,|10,9\rangle}$ and $\Delta_{|10,10\rangle,|9,9\rangle}$ (that set the bias voltages of the $\frac{d^2I}{dV^2}$ peaks) increase when a magnetic field is applied parallel to the SMM easy axis. However, in general these energy differences depend on the orientation of the magnetic field relative to the SMM easy axis and can be nonlinear [30].

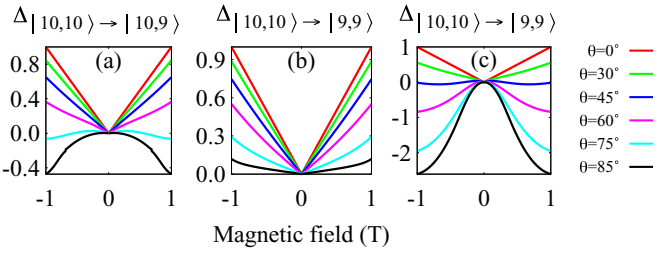

FIG. 2. (Color online) The energy difference (a) $\Delta_{|10,10\rangle,|10,9\rangle}$ and [(b), (c)] $\Delta_{|10,10\rangle,|9,9\rangle}$ as a function of the applied magnetic field calculated by numerical diagonalization of the GSH for different values of θ, the angle between the applied magnetic field and the SMM easy axis, assuming that θ and g are the same for all of the manifolds. For simplicity, the energy differences $\Delta_{|10,10\rangle,|10,9\rangle}$ and $\Delta_{|10,10\rangle,|9,9\rangle}$ are set to zero at $B = 0$ T. The parameters of the GSH are (a)–(c) $S^{\text{g}}_{\text{tot}} = 10$, $S^{\text{e}}_{\text{tot}} = 9$, $\epsilon_0 = 1$ eV, $g^{\text{g}} = g^{\text{e}} = 2$; (b) $D^{\text{g}}/\hbar^2 = D^{\text{e}}/\hbar^2 = 0.06$ meV; and (c) $D^{\text{e}}/\hbar^2 = 0.02$ meV.

Figures 2(a) and 2(b) show $\Delta_{|10,10\rangle,|10,9\rangle}$ and $\Delta_{|10,10\rangle,|9,9\rangle}$, respectively, as a function of the applied magnetic field calculated by numerical diagonalization of the giant spin Hamiltonian for different values of the tilting angle between the magnetic field and the SMM easy axis, θ. D and g are the same for all states. As shown in Fig. 2(a), $\Delta_{|10,10\rangle,|10,9\rangle}$ increases linearly as a function of the applied magnetic field parallel to the SMM easy axis (the red curve). However, at large tilting angles between the applied magnetic field and the SMM easy axis, $\Delta_{|10,10\rangle,|10,9\rangle}$ varies nonlinearly. For some tilting angles, $\Delta_{|10,10\rangle,|10,9\rangle}$ even decreases with increasing the magnetic field [e.g., the light blue curve in Fig. 2(a)].

Figure 2(b) shows $\Delta_{|10,10\rangle,|9,9\rangle}$ as a function of the applied magnetic field for various tilting angles. Although $\Delta_{|10,10\rangle,|9,9\rangle}$ depends on the tilting angle, it never becomes negative. Therefore, applying a magnetic field in any direction relative to the SMM's easy axis shifts the second $\frac{d^2I}{dV^2}$ peak to a higher voltage. However, in the experiment [5] the second $\frac{d^2I}{dV^2}$ peak shifts to a lower bias voltage upon application of the magnetic field. Thus, the GSH approach parameters selected in Fig. 1 do not reproduce the experimental results.

B. Spin manifolds with differing anisotropies

This scenario changes if different anisotropy constants are chosen for different manifolds of the neutral SMM. Figure 2(c) shows $\Delta_{|10,10\rangle,|9,9\rangle}$ as a function of the applied magnetic field for different values of θ and a different set of parameters. For this set of parameters, it is assumed that the anisotropy of the excited-state manifold, $D^{\text{e}}/\hbar^2 = 0.02$ meV, is smaller than the anisotropy of the ground-state manifold, $D^{\text{g}}/\hbar^2 = 0.06$ meV. However, the magnetic g factors are the same for all of the spin manifolds.

As shown in Fig. 2(c), at the tilting angle $\theta = 60^\circ$ the energy difference that corresponds to the second peak, $\Delta_{|10,10\rangle,|9,9\rangle}$, is decreased by applying the magnetic field. However, the energy difference that corresponds to the first peak, $\Delta_{|10,10\rangle,|10,9\rangle}$, increases as a function of the applied magnetic field. This

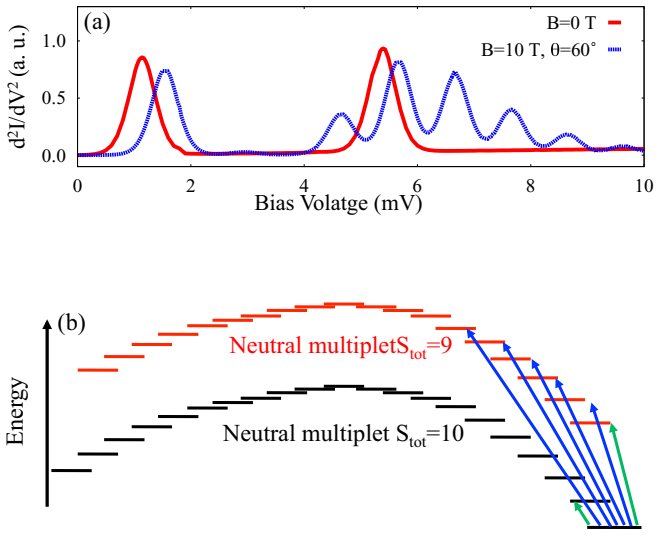

FIG. 3. (Color online) (a) Second derivative of the current, $\frac{d^2I}{dV^2}$, through the Mn_{12} SMM as a function of the bias voltage. The red (blue) curve represents $\frac{d^2I}{dV^2}$ at the applied magnetic field $B = 0$ T ($B = 10$ T with $\theta = 60^\circ$). In this calculation the neutral SMM has two manifolds. The parameters of the GSH are as in Fig. 2(c). (b) Schematic diagram representing the energies of the two manifolds of the neutral SMM ($S_{tot} = 10$ and $S_{tot} = 9$) under an applied magnetic field. The green arrows show the allowed transitions from the ground state of the ground-state manifold when the applied magnetic field is parallel to the SMM easy axis. The blue arrows show the additional allowed transitions from the ground state of the ground-state manifold when the applied magnetic field is not parallel to the SMM easy axis.

opposite behavior of $\Delta_{|10,10\rangle,|9,9\rangle}$ and $\Delta_{|10,10\rangle,|10,9\rangle}$ results in the promising behavior of $\frac{d^2I}{dV^2}$ peaks under applied magnetic field in relation to the experiment [5]. Similar behavior can be obtained for other values of the excited manifold anisotropy constants if $D^e < D^g$ for suitably chosen angles between the magnetic field direction and the magnetic easy axis of the SMM.

Figure 3(a) shows the second derivative of the current as a function of the bias voltage with the same parameters as in Fig. 2(c). As can be seen, applying a magnetic field with the tilt angle $\theta = 60^\circ$ shifts the first peak to the higher bias voltage. However, the second peak is transformed into a set of peaks in the $\frac{d^2I}{dV^2}$ plot. Here the first peak of this set is indeed shifted to a lower bias voltage in comparison to the second peak at $B = 0$ T. However, the other peaks of the manifold are not.

The appearance of the extra peaks in the $\frac{d^2I}{dV^2}$ plot can be explained as follows. When the applied magnetic field is not parallel to the SMM easy axis, S_z is not a good quantum number anymore. Thus, the tilted applied magnetic field will change the selection rule governed by the allowed transitions between the states. Under the $\Delta S_z = 0, \pm 1$ cotunneling selection rule for the GSH at zero magnetic field, the only allowed cotunneling transitions from the ground state of the neutral ground-state manifold are to the excited state of the neutral ground-state manifold ($|10,10\rangle \rightarrow |10,9\rangle$) and to the ground state of the excited-state manifold ($|10,10\rangle \rightarrow |9,9\rangle$) [the green arrows in Fig. 3(b)]. The symmetry breaking due to the magnetic field makes the transitions between the ground state of the neutral ground state and other states possible [the blue arrows in Fig. 3(b)]. These transitions have higher energies than the transition between the ground state of the neutral ground-state manifold and the ground state of the excited-state manifold resulting in the appearance of other peaks at higher bias voltages. However, no such splitting of the second peak is seen in the experimental $\frac{d^2I}{dV^2}$ plot [5] upon the application of the magnetic field.

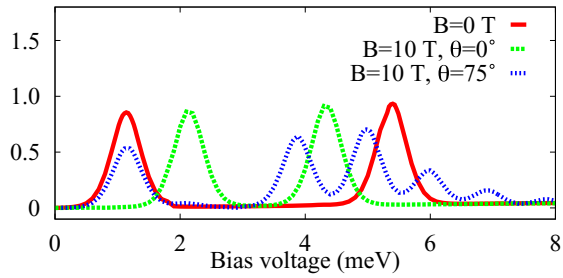

FIG. 4. (Color online) Second derivative of the current, $\frac{d^2I}{dV^2}$, of the Mn_{12} SMM as a function of the bias voltage calculated based on the GSH assuming different values of the g factor for the ground- and excited-state manifolds. The red curve represents $\frac{d^2I}{dV^2}$ at the applied magnetic field $B = 0$ T. The green (blue) curve represents $\frac{d^2I}{dV^2}$ at the applied magnetic field $B = 10$ T parallel to the SMM easy axis ($B = 10$ T with a $\theta = 75^\circ$). θ is the tilting angle between the applied magnetic field and the SMM easy axis. The parameters of the GSH are as in Fig. 1 except that $g^g/g^e = 1.2$.

In this context, it is worth pointing out that, to our knowledge, the anisotropy constants of excited SMM spin manifolds of neutral SMMs have not been measured experimentally, although experimental evidence is available [31] that indicates that the anisotropy constant of an SMM is sensitive to the SMM's charge state.

C. Spin manifolds with differing *g* factors

The opposite behavior of the $\Delta_{|10,10\rangle,|9,9\rangle}$ and $\Delta_{|10,10\rangle,|10,9\rangle}$ peaks with applied magnetic field is also reproduced if the different spin manifolds of the neutral SMM have differing g factors.

Figure 4 shows the second derivative of the current as a function of the bias voltage with the same GSH parameters as in Fig. 2 ($D^g = D^e = 0.06$) except for the g factor. In this case it is assumed that the excited-state manifold has a different g factor than that of the ground-state manifold ($g^e/g^g = 1.2$). With these GSH parameters, the magnetic field shifts the first $\frac{d^2I}{dV^2}$ peak to a higher bias voltage and shifts the second $\frac{d^2I}{dV^2}$ peak to a lower voltage which is consistent with the experimental measurement. If the magnetic field is parallel to the easy axis of the SMM these shifts are not accompanied by any splitting of the $\frac{d^2I}{dV^2}$ peaks, consistent with the experiment [5]. We found similar behavior for other values of g^e provided that $g^e/g^g > 1.12$. However, if the magnetic field is tilted strongly relative to the easy axis there is a strong splitting of the second $\frac{d^2I}{dV^2}$ peak, as can be seen in Fig. 4 for the case $\theta = 75^\circ$.

In a recent DFT calculation it has been found that the Mn_{12} SMM adsorbs with its easy axis almost perpendicular to a Bi surface, i.e., the easy axis is tilted by only 6° from the

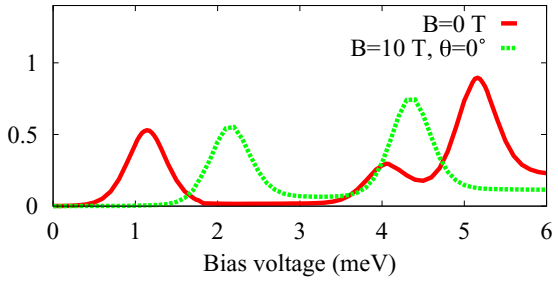

FIG. 5. (Color online) Calculated second derivative of the current, $\frac{d^2I}{dV^2}$, through the Mn_{12} SMM as a function of the bias voltage for $B = 0$ and 10 T. The magnetic field is parallel to the magnetic easy axis and the parameters of the GSH are as in Fig. 4 except that $\gamma_R/\gamma_L = 10^{-2}$.

surface normal [32]. In Kahle's experiment the magnetic field was applied perpendicularly to the surface; however, the SMM was on a BN substrate. Thus the question whether the SMM easy axis was approximately parallel to the magnetic field in the experiment remains open. If indeed the magnetic field was aligned with the easy axis, then the experimental data obtained by Kahle *et al.* [5] would lend support to the possibility that the Mn_{12} SMM manifolds have differing g factors. To our knowledge there have been no previous experimental or theoretical estimates of the g factors of excited SMM spin manifolds.

D. Weaker features in the differential conductance spectra

As has already been mentioned, for the results presented above the coupling parameters γ_R and γ_L between the molecule and the source and drain electrodes were chosen in such a way that the population of the excited states of the ground state spin manifold of the SMM was always very small. Thus transitions between the excited states of the ground-state spin manifold and states of the excited state manifold did not result in visible features in the calculated $\frac{d^2I}{dV^2}$ spectra. In Fig. 5 we show calculated $\frac{d^2I}{dV^2}$ spectra for a different choice of coupling parameter ratio ($\gamma_R/\gamma_L = 10^{-2}$) that allows significant occupation of the first excited state $|10,9\rangle$ of the ground-state spin manifold. Transitions $|10,9\rangle \rightarrow |9,9\rangle$ between this state and the lowest state $|9,9\rangle$ of the excited spin manifold then have a visible impact on the calculated $\frac{d^2I}{dV^2}$ spectra, giving rise to the peak at $V_{\rm bias} = 4$ mV for $B = 0$ in Fig. 5. This peak falls between the previously discussed $\frac{d^2I}{dV^2}$ peaks that are due to transitions $|10,10\rangle \rightarrow |10,9\rangle$ and $|10,10\rangle \rightarrow |9,9\rangle$ that are seen for $B = 0$ at bias voltages $\sim$ 1.2 and 5.2 mV, respectively, in Fig. 5. It resembles the weak features seen between the main $\frac{d^2I}{dV^2}$ peaks in the experimental data of Kahle *et al.* [5] at $B = 0$. Like those weak features in the data of Kahle *et al.* [5] the weak $\frac{d^2I}{dV^2}$ peak is no longer visible in Fig. 5 at $B = 10$ T. The reason for its disappearance is that (as expected for a $|10,9\rangle \rightarrow |9,9\rangle$ transition) it shifts to lower bias voltages with increasing B faster than does the peak due to the $|10,10\rangle \rightarrow |9,9\rangle$ transition and at 10 T is obscured by the stronger peak due to the $|10,10\rangle \rightarrow |10,9\rangle$ transition that is located at $V_{\rm bias} = 2.2$ mV at $B = 10$ T.

Since the $|10,9\rangle \rightarrow |9,9\rangle$ transition occurs between states having the same value of S_z but belonging to two different spin manifolds, the weak differential conductance feature associated with this transition is predicted to shift with the magnetic field by amounts proportional to $\Delta g = g^{\rm g} - g^{\rm e}$. Therefore, an experimental measurement of the weak feature's location as a function of the magnetic field could, in principle, result in a direct experimental estimate of Δg and thus of the g factor of the SMM's excited spin manifold.

IV. CONCLUSIONS

In summary, we have presented the following two scenarios as possible causes of the experimentally observed [5] opposite behaviors of the two low energy excitations of the Mn_{12} SMM under applied magnetic field: (i) The applied magnetic field is not parallel to the SMM's easy axis and the spin-state manifolds of the neutral SMM have different anisotropy constants. (ii) The applied magnetic field is parallel to the SMM's easy axis; however, the spin-state manifolds of the neutral SMM have different g factors. Both of these scenarios indicate that the first excited-state manifold of the neutral Mn_{12} SMM has different properties in comparison with its ground-state manifold and both can account for the low bias peaks in the cotunneling spectra moving in opposite directions with the applied magnetic field, as was observed experimentally [5]. However, in the first scenario a $\frac{d^2I}{dV^2}$ peak splitting that was not observed experimentally is predicted. Thus the second scenario accounts better for the experimental data. We attribute the strong features in the cotunneling spectra of Kahle *et al.* [5] to transitions from the ground state of the ground-state spin manifold of the SMM to other states of the ground-state manifold and states of exited manifolds. Transitions from excited states of the ground-state manifold give rise to differential conductance features whose properties resemble those of the weaker features in the cotunneling spectra of Kahle *et al.* [5].

Further experimental results are needed to better identify the unique Hamiltonian parameters of the excited-state manifolds of the neutral SMM. We hope that this investigation will stimulate further experimental and theoretical studies.

ACKNOWLEDGMENTS

This research was supported by CIFAR, NSERC, Westgrid, and Compute Canada. We thank B. Gates and B. L. Johnson for helpful comments and discussions.

[1] H. B. Heersche, Z. de Groot, J. A. Folk, H. S. J. van der Zant, C. Romeike, M. R. Wegewijs, L. Zobbi, D. Barreca, E. Tondello, and A. Cornia, Phys. Rev. Lett. **96**, 206801 (2006).

[2] M.-H. Jo, J. E. Grose, K. Baheti, M. M. Deshmukh, J. J. Sokol, E. M. Rumberger, D. N. Hendrickson, J. R. Long, H. Park, and D. C. Ralph, Nano Lett. **6**, 2014 (2006).

[3] A. S. Zyazin, J. W. G. van den Berg, E. A. Osorio, H. S. J. van der Zant, N. P. Konstantinidis, M. Leijnse, M. R. Wegewijs, F. May, W. Hofstetter, C. Danieli, and A. Cornia, Nano Lett. **10**, 3307 (2010).
[4] M. Urdampilleta, S. Klyatskaya, J-P. Cleuziou, M. Ruben, and W. Wernsdorfer, Nat. Mater. **10**, 502 (2011).
[5] S. Kahle, Z. Deng, N. Malinowski, C. Tonnoir, A. Forment-Aliaga, N. Thontasen, G. Rinke, D. Le, V. Turkowski, T. S. Rahman, S. Rauschenbach, M. Ternes, and K. Kern, Nano Lett. **12**, 518 (2012).
[6] G.-H. Kim and T.-S. Kim, Phys. Rev. Lett. **92**, 137203 (2004).
[7] C. Romeike, M. R. Wegewijs, and H. Schoeller, Phys. Rev. Lett. **96**, 196805 (2006).
[8] C. Timm, Phys. Rev. B **76**, 014421 (2007).
[9] M. Misiorny, I. Weymann, and J. Barnas, Phys. Rev. B **79**, 224420 (2009).
[10] H.-Z. Lu, B. Zhou, and S.-Q. Shen, Phys. Rev. B **79**, 174419 (2009).
[11] K. Park and M. R. Pederson, Phys. Rev. B **70**, 054414 (2004).
[12] S. Barraza-Lopez, K. Park, V. García-Suárez, and J. Ferrer, J. Appl. Phys. **105**, 07E309 (2009).
[13] S. Barraza-Lopez, K. Park, V. García-Suárez, and J. Ferrer, Phys. Rev. Lett. **102**, 246801 (2009).
[14] C. D. Pemmaraju, I. Rungger, and S. Sanvito, Phys. Rev. B **80**, 104422 (2009).
[15] Ł. Michalak, C. M. Canali, M. R. Pederson, M. Paulsson, and V. G. Benza, Phys. Rev. Lett. **104**, 017202 (2010).
[16] K. Park, S. Barraza-Lopez, V. M. García-Suárez, and J. Ferrer, Phys. Rev. B **81**, 125447 (2010).
[17] F. Rostamzadeh Renani and G. Kirczenow, Phys. Rev. B **85**, 245415 (2012).
[18] F. Rostamzadeh Renani and G. Kirczenow, Phys. Rev. B **84**, 180408(R) (2011).
[19] F. Rostamzadeh Renani and G. Kirczenow, Phys. Rev. B **87**, 121403 (2013).
[20] T. Lis, Acta Crystallogr., Sect. B: Struct. Crystallogr. Cryst. Chem. **36**, 2042 (1980)
[21] A. Caneschi, D. Gatteschi, R. Sessoli, A. L. Barra, L. C. Brunel, and M. Guillot, J. Am. Chem. Soc. **113**, 5873 (1991).
[22] A. L. Barra, D. Gatteschi, and R. Sessoli, Phys. Rev. B **56**, 8192 (1997).
[23] V. S. Zagaynova, T. L. Makarova, N. G. Spitsina, and D. W. Boukhvalov, J. Supercond. Novel Magn. **24**, 855 (2011).
[24] R. Sessoli, D. Gatteschi, A. Caneschi, and M. A. Novak, Nature (London) **365**, 141 (1993).
[25] A. A. Mukhin, V. D. Travkin, A. K. Zvezdin, S. P. Lebedev, A. Caneschi, and D. Gatteschi, Europhys. Lett. **44**, 778 (1998).
[26] A. M. Gomes, M. A. Novak, R. Sessoli, A. Caneschi, and D. Gatteschi, Phys. Rev. B **57**, 5021 (1998).
[27] K. Park, M. R. Pederson, and C. S. Hellberg, Phys. Rev. B **69**, 014416 (2004).
[28] For a review, see G. Kirczenow, in *The Oxford Handbook of Nanoscience and Technology, Volume I: Basic Aspects*, edited by A. V. Narlikar and Y. Y. Fu (Oxford University Press, Oxford, 2010), Chap. 4.7.1.
[29] A. Cornia, R. Sessoli, L. Sorace, D. Gatteschi, A. L. Barra, and C. Daiguebonne, Phys. Rev. Lett. **89**, 257201 (2002).
[30] E. Burzuri, A. S. Zyazin, A. Cornia, and H. S. J. van der Zant, Phy. Rev. Lett. **109**, 147203 (2012).
[31] M. Soler, W. Wernsdorfer, K. A. Abboud, J. C. Huffman, E. R. Davidson, D. N. Hendrickson, and G. Christou, J. Am. Chem. Soc. **125**, 3576 (2003).
[32] K. Park and J.-Z. Wang, Polyhedron **66**, 157 (2013).